CMS Physics Analysis Summary

Contact: cms-pag-conveners-higgs@cern.ch 2018/02/28

Search for the exotic decay of the Higgs boson to a pair of light pseudoscalars in the final state with two b quarks and two τ leptons

The CMS Collaboration

Abstract

A search for the exotic decay of the Higgs boson to a pair of light pseudoscalar bosons is performed in the final state with two b jets and two τ leptons. The motivation lies in models beyond the standard model (SM), such as two-Higgs-doublet models extended with a complex scalar singlet, which include the next-to-minimal supersymmetric SM (NMSSM). The results are based on an integrated luminosity of 35.9 fb^{-1}, accumulated by the CMS experiment at the LHC in 2016 at 13 TeV center-of-mass energy. Masses of the pseudoscalar boson between 15 and 60 GeV are probed, and upper limits as low as 23% are set on the branching fraction of the Higgs boson to two light pseudoscalar bosons in the NMSSM, assuming that the production cross section of the Higgs boson is the one predicted in the SM. No mass constraint is set on the b jet pair, making this search sensitive to Higgs boson decays to two scalars with different masses.

1 Introduction

Within the standard model (SM), the Brout-Englert-Higgs mechanism [1–6] is responsible for electroweak symmetry breaking, and predicts the existence of a massive scalar particle, the Higgs boson. A particle compatible with the Higgs boson was discovered by the ATLAS and CMS Collaborations at the CERN LHC [7–9]. Measurements of the couplings and properties of this particle leave room for exotic decays, with a limit of 34% on the branching fraction of the Higgs boson to beyond the SM (BSM) particles at the 95% confidence level (CL), using data collected at a center-of-mass energy of 8 TeV [10, 11].

The possible existence of exotic decays of the Higgs boson is well motivated [12–15]. The width of the Higgs boson in the SM is so narrow that a small coupling to a light state could lead to branching fractions of the Higgs boson to that light state of the order of several percent. Additionally, the scalar sector can theoretically easily be a portal that allows matter from a hidden sector to interact with SM particles. In general, exotic decays of the Higgs boson are allowed in many models that are consistent with all the LHC measurements published so far.

An interesting class of exotic Higgs boson decays consists in decays to a pair of light pseudoscalars, which then decay to pairs of SM particles. The minimal supersymmetric SM (MSSM) cannot accomodate such decays with all the measurements performed at the LHC [16–22]. This type of process is however still allowed in various other models, including two Higgs doublet models augmented by a scalar singlet (2HDM+S). Seven scalar and pseudoscalar particles are predicted in 2HDM+S. One of them, h, can be a scalar compatible with the discovered particle with a mass of 125 GeV, and another one is a pseudoscalar, a, light enough that $\mathrm{h} \to \mathrm{aa}$ decays are allowed.

Four types of 2HDM, and by extension 2HDM+S, forbid flavor changing neutral currents (FCNC) at tree level [23]. In type I, all SM particles couple to the first doublet. In type II, leptons and down-type quarks couple to the second doublet, whereas up-type quarks couple to the first doublet. The next-to-minimal supersymmetric model (NMSSM) is a particular case of 2HDM+S of type II that brings a solution to the μ problem [24]. In type III, leptons couple to the second doublet, and quarks to the first one. Finally, in type IV, down-type quarks couple to the second doublet, while leptons and up-type quarks couple to the first doublet [15]. The branching fractions of the light pseudoscalars to pairs of SM particles depend on the type of 2HDM+S, on the pseudoscalar mass m_a, and on $\tan\beta$, defined as the ratio of the vacuum expectation value of the second and first doublet. The value of $\mathcal{B}(\mathrm{aa} \to \mathrm{bb}\tau\tau)$ is slightly above 10% in the NMSSM — or more generally 2HDM+S type II — for $\tan\beta > 1$, and can reach up to about 50% in 2HDM+S type III with $\tan\beta \sim 2$, as shown in Fig. 1.

Several searches for exotic decays of the Higgs boson to a pair of light pseudoscalar bosons have been performed by the CMS Collaboration with data collected at a center-of-mass energy of 8 TeV in different final states: 2μ2b for $25 < m_\mathrm{a} < 62.5$ GeV [25], $2\mu2\tau$ for $15 < m_\mathrm{a} < 62.5$ GeV [25], 4τ for $4 < m_\mathrm{a} < 8$ GeV [26] and $5 < m_\mathrm{a} < 15$ GeV [25], and 4μ for $0.25 < m_\mathrm{a} < 3.5$ GeV [27]. The ATLAS Collaboration reported results for the following final states: 4b for $20 < m_\mathrm{a} < 60$ GeV [28]; 4μ, 4e, and 2e2μ for $15 < m_\mathrm{a} < 60$ GeV at 8 TeV center-of-mass energy [29] and for $1 < m_\mathrm{a} < 60$ GeV at 13 TeV center-of-mass energy [30]; 4γ for $10 < m_\mathrm{a} < 62$ GeV [31]; and $2\mu2\tau$ for $3.7 < m_\mathrm{a} < 50$ GeV [32]. The 2b2τ final state has so far never been probed. This final state benefits from large branching fractions in most models because of the large mass of τ leptons and b quarks with respect to other leptons and quarks. The presence of light leptons originating from the τ decays allows triggering events in the dominant gluon fusion production mode.

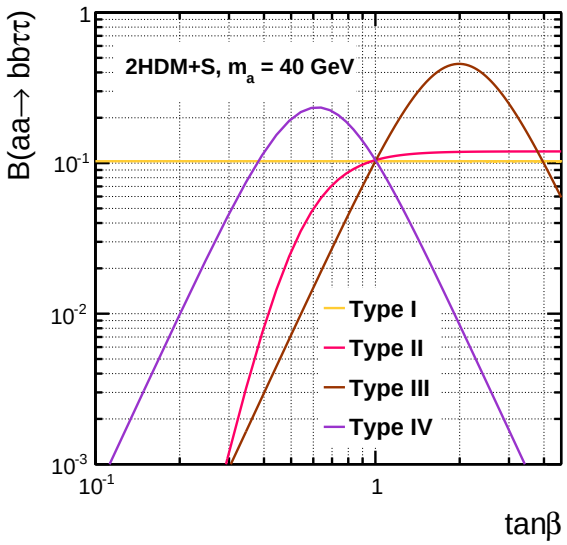

Figure 1: Predicted $\mathcal{B}(aa \to bb\tau\tau)$ for $m_a = 40$ GeV in the different models of 2HDM+S, for various values of $\tan\beta$. The picture is essentially the same for all m_a hypotheses considered in this paper. The branching fractions are computed following the formulae in Ref. [15].

This letter reports on the search with the CMS experiment for exotic decays of the Higgs boson to a pair of light pseudoscalar bosons, in the final state with two τ leptons and two bottom quarks. Masses of the pseudoscalar boson between 15 and 60 GeV are probed. Between twice the b quark mass and 15 GeV, the τ leptons and the b jets become collimated, which would necessitate the use of boosted reconstruction techniques. The search is based on proton-proton (pp) collision data collected at a center-of-mass energy of 13 TeV and corresponding to an integrated luminosity of 35.9 fb^{-1}. Throughout this letter, the term τ_h denotes τ leptons decaying hadronically. The di-τ final states studied in this search are eμ, eτ_h, and $\mu\tau_\text{h}$. Despite its large branching fraction, the $\tau_\text{h}\tau_\text{h}$ final state is not considered because the signal acceptance after the trigger requirements would be negligible. The ee and $\mu\mu$ final states for the di-τ lepton pair have a low branching fraction, and suffer from a large contribution of Drell-Yan background events with prompt decays to electrons and muons.

2 The CMS detector

The central feature of the CMS apparatus is a superconducting solenoid of 6 m internal diameter, providing a magnetic field of 3.8 T. Within the solenoid volume, there are a silicon pixel and strip tracker, a lead tungstate crystal electromagnetic calorimeter (ECAL), and a brass and scintillator hadron calorimeter (HCAL), each composed of a barrel and two endcap sections. Forward calorimeters extend the pseudorapidity coverage provided by the barrel and endcap detectors. Muons are detected in gas-ionization chambers embedded in the steel flux-return yoke outside the solenoid.

Events of interest are selected using a two-tiered trigger system [33]. The first level, composed of custom hardware processors, uses information from the calorimeters and muon detectors to select events at a rate of around 100 kHz within a time interval of less than 4 μs. The second level, known as the high-level trigger, consists of a farm of processors running a version of the full event reconstruction software optimized for fast processing, and reduces the event rate to

about 1 kHz before data storage.

A more detailed description of the CMS detector, together with a definition of the coordinate system used and the relevant kinematic variables, can be found in Ref. [34].

3 Simulated samples and event reconstruction

The signal and some of the background processes are modeled with samples of simulated events. The MG5_aMC@NLO [35] generator is used for the $h \to aa \to 2\tau 2b$ signal process, in gluon fusion (ggh), vector boson fusion (VBF), or associated vector boson (Wh, Zh) processes. These samples are simulated at leading order (LO) in perturbative quantum chromodynamics (pQCD) with the MLM jet matching and merging [36]. The $Z + jets$ and $W + jets$ processes are also generated with the MG5_aMC@NLO generator at LO with the MLM jet matching and merging. The FxFx merging scheme is used to generate diboson background with the MG5_aMC@NLO generator at NLO. The $t\bar{t}$ process is generated at NLO with the POWHEG 2.0 [37–41] generator. The single top quark samples are produced at NLO with the POWHEG 1.0 generator. Backgrounds from SM Higgs boson production are generated at NLO with the POWHEG 2.0 generator, and the MINLO HVJ [42] extension of POWHEG 2.0 is used for the WH and ZH simulated samples. The generators are interfaced with PYTHIA 8.212 [43] to model the parton showering and fragmentation, as well as the decay of the τ leptons. The CUETP8M1 tune [44] is chosen for the PYTHIA parameters affecting the description of the underlying event. The set of parton distribution functions (PDFs) is NLO NNOPDF3.0 for NLO samples, and LO NNPDF3.0 for LO samples.

The full NNLO plus next-to-next-to-leading-log (NNLL) order calculation [45], performed with the TOP++ 2.0 program [46], is used to compute the $t\bar{t}$ cross section. The PDF uncertainty is estimated using the PDF4LHC prescription [47, 48] with the MSTW2008, CT10 NNLO [49, 50], and NNPDF2.3 5f FFN [51] PDF sets, and added in quadrature to the uncertainty associated to the strong coupling constant (α_s) to obtain a $t\bar{t}$ production cross section of 832^{+20}_{-29}(scale)$\pm$35(PDF+α_s) pb assuming m_t=172.5 GeV.

During the 2016 data-taking period at the LHC, the average number of pp interactions per bunch crossing was about 27. All simulated samples include additional pp interactions per bunch crossing, referred to as "pileup", obtained by generating concurrent minimum bias collision events using PYTHIA. The simulated events are reweighted in such a way to have the same pileup distribution as data. Generated events are processed through a simulation of the CMS detector based on GEANT4 [52].

The reconstruction of events relies on the particle-flow (PF) algorithm [53], which combines the information from the CMS subdetectors to identify and reconstruct the particles emerging from pp collisions: charged hadrons, neutral hadrons, photons, muons, and electrons. Combinations of these PF objects are used to reconstruct higher-level objects such as jets, τ_h candidates and missing transverse momentum. The reconstructed vertex with the largest value of summed physics-object p_T^2 is taken to be the primary pp interaction vertex. The physics objects are the objects constructed by a jet finding algorithm [54, 55] applied to all charged tracks associated with the vertex, and the corresponding associated missing transverse momentum.

Jets are reconstructed from PF objects with the anti-k_T clustering algorithm implemented in the FASTJET library [55, 56], using a distance parameter of 0.4. Corrections to the jet energy are applied as a function of the p_T and η of the jet [57]. The jets in this search are required to be separated from the selected leptons by $\Delta R \geq 0.5$. Jets that originate from b quarks,

called b jets, are identified with the combined secondary vertex (CSV) algorithm [58]. The CSV algorithm builds a discriminant from variables related to potential secondary vertices associated to the jet, and from track-based lifetime information. The working point chosen in this search provides an efficiency of about 70%, and a misidentification rate for light flavor and quark jets of approximately 1%.

The missing transverse momentum, $\vec{p}_{\mathrm{T}}^{\,\mathrm{miss}}$, is defined as the negative vectorial sum of the transverse momenta of all PF objects reconstructed in the event. The magnitude of this vector is denoted $p_{\mathrm{T}}^{\mathrm{miss}}$.

Hadronically decaying τ leptons, denoted τ_{h}, are reconstructed with the Hadrons-Plus-Strips (HPS) algorithm [59, 60] as a combination of tracks and energy deposits in strips of the ECAL. The tracks reconstruct the charged hadrons, and the strips the neutral pions, which decay to a pair of photons with potential electron-positron conversion. The reconstructed τ_{h} decay modes are 1 track, 1 track plus at least one strip, and 3 tracks. The rate for jets to be misidentified as τ_{h} is reduced by applying an MVA discriminator that uses isolation as well as lifetime variables. The working point of the discriminator chosen in this analysis has an efficiency of about 60%, for a misidentification rate of light flavor jets of the order of 0.4%. Additionally, discriminators that reduce the rates with which electrons and muons are misidentified as τ_{h} are applied. Loose working points with an efficiency above 90% are chosen because the $\mathrm{Z} \to \mathrm{ee}/\mu\mu$ background does not contribute much in the region where the signal is expected.

Electrons are reconconstructed by matching ECAL clusters to tracks in the tracker. They are then identified with a multivariate (MVA) discriminant that makes use of variables related to energy deposits in the ECAL, the quality of the track, and the compatibility between the ECAL clusters and the track that have been matched together [61]. The working point chosen in this search has an efficiency of about 80%. Two algorithms are used to reconstruct muons: the first one is based on the reconstruction of a track from hits in the tracker and in the muon system, while the second one matches a track from the tracker to hits in the muon system. Muons are then identified on the basis of the track reconstruction quality and on the number of measurements in the tracker and the muon systems [62]. The relative isolation of electrons and muons is defined as:

$$I^{\ell} \equiv \frac{\sum_{\text{charged}} p_{\mathrm{T}} + \max\left(0, \sum_{\text{neutral}} p_{\mathrm{T}} - \frac{1}{2}\sum_{\text{charged, PU}} p_{\mathrm{T}}\right)}{p_{\mathrm{T}}^{\ell}}. \tag{1}$$

In this formula, $\sum_{\text{charged}} p_{\mathrm{T}}$ is the scalar sum of the transverse momenta of the charged particles associated to the primary vertex and in a cone around the lepton direction, with size $\Delta R = \sqrt{(\Delta\eta)^2 + (\Delta\phi)^2} = 0.4$ for muons, or 0.3 for electrons. The sum $\sum_{\text{neutral}} p_{\mathrm{T}}$ represents a similar quantity for neutral particles. As estimated from simulation, the p_{T} of neutral particles from pileup vertices is about half of that of charged hadrons associated to pileup vertices, denoted by $\sum_{\text{charged, PU}} p_{\mathrm{T}}$. The p_{T} of the lepton is denoted p_{T}^{ℓ}.

4 Selection

Events are selected in three different $\tau\tau$ final states: $\mathrm{e}\mu$, $\mathrm{e}\tau_{\mathrm{h}}$, and $\mu\tau_{\mathrm{h}}$. These events should in addition contain one b jet. The dominant backgrounds with these objects in the final state are $\mathrm{t\bar{t}}$ and $\mathrm{Z} \to \tau\tau$. Events with jets misidentified as electrons, muons, or electrons, such as W +jets, QCD multijet, or semi-leptonic $\mathrm{t\bar{t}}$ events, contribute to a non negligible fraction of the background as well.

Table 1: Baseline selection criteria on the objects selected in the various final states. The numbers given for the p_T thresholds of the electron and muon in the eμ correspond to a combination of asymmetric electron-plus-muon triggers. The p_T threshold for the τ_h candidates is the result of an optimization of the expected exclusion limits of the signal.

	$\mu\tau_h$	$e\tau_h$	$e\mu$
$p_T(\tau_h)$	> 25 GeV	> 25 GeV	-
$p_T(\mu)$	> 20 GeV	-	$> 24/13$ GeV
$p_T(e)$	-	> 26 GeV	$> 13/24$ GeV
$p_T(b)$	> 20 GeV	> 20 GeV	> 20 GeV
$\lvert\eta(\tau_h)\rvert$	< 2.3	< 2.3	-
$\lvert\eta(\mu)\rvert$	< 2.1	-	< 2.4
$\lvert\eta(e)\rvert$	-	< 2.1	< 2.4
$\lvert\eta(b)\rvert$	< 2.4	< 2.4	< 2.4
Isolation (τ_h)	MVA	MVA	-
Isolation (μ)	< 0.15	-	< 0.15
Isolation (e)	-	< 0.10	< 0.10

All events are required to have at least one b-tagged jet with $p_T > 20$ GeV and $|\eta| < 2.4$. About 90% of signal events passing this condition only have one such jet, as a result of the typically soft b jet p_T spectrum and of the inefficiency of the b-tagging algorithm. Events in the $\mu\tau_h$ final state are selected with a combination of triggers requiring an isolated muon, or a muon and a τ_h candidate. In the $e\tau_h$ final state, the trigger is based on the presence of an isolated electron, whereas in the eμ final state, it is based on the presence of both an electron and a muon. The leptons and τ_h are required to be well identified and isolated, to have opposite charge, and to be separated by at least $\Delta R = 0.4$ if there is a τ_h, or 0.3 otherwise. Table 1 details the p_T, η, isolation, and identification criteria for the various objects, in the different final states. The isolation and separation conditions make this search insensitive to signals with very low m_a ($2m_b < m_a < 15\,\text{GeV}$), which are characterized by collimated decay products of the pseudoscalar bosons.

To increase the sensitivity of the analysis, events in each final state are separated into four categories with different signal-to-background ratios. The categories are defined on the basis of the visible invariant mass of the τ leptons and of the b-tagged jet with the highest p_T, denoted $m^{vis}_{b\tau\tau}$. This variable is typically low for signal events because the three objects come from a 125 GeV Higgs boson, but it is on average much larger for background events, where the three objects do not come from a resonant decay. The distribution of $m^{vis}_{b\tau\tau}$ for different m_a hypotheses is shown in Fig. 2 for the $\mu\tau_h$ final state. The thresholds that define the categories are indicated in Table 2, and depend on the di-τ lepton final state: they are lower in the eμ final state because there are more neutrinos not included in the mass calculation, and they are higher in the $e\tau_h$ final state to keep enough events despite the lower signal acceptance related to the electron p_T thresholds. Signal samples with high m_a contribute mostly to the first two categories, whereas those with low m_a are concentrated in the second and third categories. The last category is almost signal-free and has large background yields; it is useful to constrain the various backgrounds and provides some additional sensitivity for low m_a signal samples. The background proportion in the categories strongly increases with $m^{vis}_{b\tau\tau}$. The results of the search are extracted from a fit of the visible di-τ mass ($m^{vis}_{\tau\tau}$) distributions in each of the categories, because this is a resonant distribution for signal events. The variables $m^{vis}_{\tau\tau}$ and $m^{vis}_{b\tau\tau}$ are partially correlated.

Selection criteria are applied to optimize the expected limits on the signal cross section times

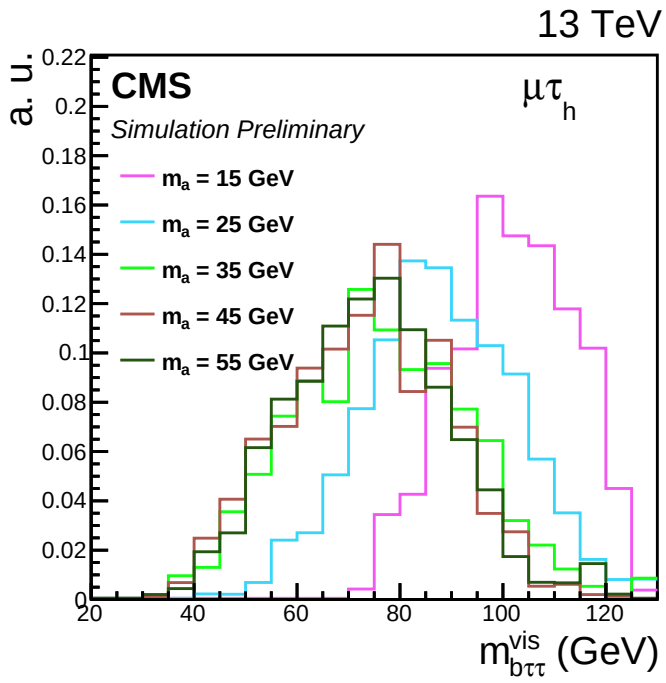

Figure 2: Visible invariant mass of the leptons and the leading b jet, $m^{\text{vis}}_{\text{b}\tau\tau}$, after the baseline selection, in the $\mu\tau_{\text{h}}$ final state.

branching fraction. They are based on the transverse mass of the $\vec{p}_{\text{T}}^{\,\text{miss}}$ and the leptons, m_{T}, and on D_ζ. The transverse m_{T} between a lepton ℓ and the $\vec{p}_{\text{T}}^{\,\text{miss}}$ is defined as

$$m_{\text{T}}(\ell, \vec{p}_{\text{T}}^{\,\text{miss}}) \equiv \sqrt{2 p_{\text{T}}^{\ell} p_{\text{T}}^{\text{miss}} [1 - \cos(\Delta\phi)]}, \tag{2}$$

where p_{T}^{ℓ} is the transverse momentum of the lepton ℓ, and $\Delta\phi$ is the azimuthal angle between its direction and the $\vec{p}_{\text{T}}^{\,\text{miss}}$. Selecting events with low m_{T} strongly reduces the backgrounds from W + jets and $\text{t}\bar{\text{t}}$ events, which are characterized by a larger $\vec{p}_{\text{T}}^{\,\text{miss}}$. In addition, for W + jets events where the selected lepton comes from the W boson decay, the invariant mass of the neutrino, approximated by $\vec{p}_{\text{T}}^{\,\text{miss}}$ in the transverse plane, and of the lepton, is expected to be resonant at high m_{T}. The variable D_ζ is defined as

$$D_\zeta \equiv p_\zeta - 0.85\, p_\zeta^{\text{vis}}, \tag{3}$$

where p_ζ is the component of the $\vec{p}_{\text{T}}^{\,\text{miss}}$ along the bisector of the transverse momenta of the two τ candidates and p_ζ^{vis} is the sum of the components of the lepton transverse momenta along the same direction [63]. The $\text{Z} \to \tau\tau$ background typically has large D_ζ values because $\vec{p}_{\text{T}}^{\,\text{miss}}$ is approximately collinear to the $\tau\tau$ system, whereas the $\text{t}\bar{\text{t}}$ background is concentrated at lower D_ζ values because of typically large $\vec{p}_{\text{T}}^{\,\text{miss}}$ not aligned with the $\tau\tau$ system. The signal lies in an intermediate region because $\vec{p}_{\text{T}}^{\,\text{miss}}$ is approximately aligned with the $\tau\tau$ system, but $p_{\text{T}}^{\text{miss}}$ is usually small. The precise criteria per final state and category are indicated in Table 2.

5 Background estimation

The $\text{Z} \to \ell\ell$ background is estimated from simulation. The distributions of the p_{T} of the dilepton system and of the visible invariant mass between the leptons and the leading b jet, are

Table 2: Optimized selection and categorization in the various final states.

Cut	Category 1	Category 2	Category 3	Category 4
	$e\mu$			
$m_{b\tau\tau}^{vis}$	< 65 GeV	$\in [65, 80]$ GeV	$\in [80, 95]$ GeV	> 95 GeV
$m_T(e, \vec{p}_T^{miss})$	< 40 GeV	< 40 GeV	< 40 GeV	< 40 GeV
$m_T(\mu, \vec{p}_T^{miss})$	< 40 GeV	< 40 GeV	< 40 GeV	< 40 GeV
D_ζ	> -30 GeV	> -30 GeV	> -30 GeV	> -30 GeV
	$e\tau_h$			
$m_{b\tau\tau}^{vis}$	< 80 GeV	$\in [80, 100]$ GeV	$\in [100, 120]$ GeV	> 120 GeV
$m_T(e, \vec{p}_T^{miss})$	< 40 GeV	< 50 GeV	< 50 GeV	< 40 GeV
$m_T(\tau_h, \vec{p}_T^{miss})$	< 60 GeV	< 60 GeV	< 60 GeV	< 60 GeV
	$\mu\tau_h$			
$m_{b\tau\tau}^{vis}$	< 75 GeV	$\in [75, 95]$ GeV	$\in [95, 115]$ GeV	> 115 GeV
$m_T(\mu, \vec{p}_T^{miss})$	< 40 GeV	< 50 GeV	< 50 GeV	< 40 GeV
$m_T(\tau_h, \vec{p}_T^{miss})$	< 60 GeV	< 60 GeV	< 60 GeV	< 60 GeV
D_ζ	-	< 0 GeV	-	-

reweighted with corrections derived in data from a region enriched in $Z \to \mu\mu + \geq 1$ b events. The simulation is separated between $Z \to \tau\tau$, where the reconstructed τ candidates correspond to τ leptons at generated level, and $Z \to ee/\mu\mu$ decays, where at least one electron or muon is misidentified.

Backgrounds with a jet misidentified as a τ_h candidate are estimated from data using the so-called fake rate method. These consist mostly of W + jets and QCD multijet events, as well as $t\bar{t}$, diboson, and single top quark production events where the reconstructed τ_h corresponds to a jet. The probabilities for jets to be misidentified as τ_h candidates, denoted f, are estimated from $Z \to \mu\mu$ + jets events in data. They are parameterized with Landau distributions as a function of the τ_h p_T, separately for every reconstructed τ_h decay mode. Events that pass all the selection criteria for the signal region, except that the τ_h candidate fails the isolation condition, are reweighted with a weight $f/(1-f)$ to estimate the contribution of events with jets in the signal region. Events with genuine τ_h, electrons, or muons, in the anti-isolated region, are estimated from simulation and subtracted from data.

In the $e\mu$ final state, the W + jets background is estimated from simulation. Such events typically have a real lepton coming from the W boson decay, and a jet misidentified as the other lepton. The QCD multijet background, which also contains jets misidentified as leptons, is estimated from data. Its normalization corresponds to the difference between the data and the sum of all the others backgrounds in a region where the τ candidates have the same sign. A smooth distribution is obtained by additionally relaxing the isolation conditions of both leptons. A correction is applied to extrapolate the normalization obtained in the same-sign region to the signal region.

Other processes, including diboson, $t\bar{t}$ and single top productions, as well as SM Higgs boson processes in various production and decay modes, are estimated from simulation. The $t\bar{t}$ production is a major background, especially in the $e\mu$ final state. The $t\bar{t}$ simulation models well the variables used in this analysis, as it has been verified in a control region in the $e\mu$ final state where no selection criterion is applied on $m_T(e, \vec{p}_T^{miss})$ nor $m_T(\mu, \vec{p}_T^{miss})$, and where the D_ζ selection criterion is inverted.

In the $e\tau_h$ and $\mu\tau_h$ final states, where all backgrounds with a jet misidentified as a τ_h candidate

are estimated from data, simulated events with a reconstructed τ_h matched to a jet at generator level are discarded to avoid double counting.

6 Fit method and systematic uncertainties

The search for an excess of signal events over the expected background involves a global maximum likelihood fit based on the $m_{\tau\tau}^{\text{vis}}$ distributions in the different channels and categories. The systematic uncertainties are represented by nuisance parameters that are varied in the fit according to their probability density function. A log-normal probability density function is assumed for the nuisance parameters affecting the event yields of the various background and signal contributions, whereas systematic uncertainties that affect the distributions are represented by nuisance parameters whose variation results in a continuous perturbation of the spectrum [64] and which are assumed to have a Gaussian probability density function.

To take into account the limited size of simulated samples and of data in the control regions used to estimate some of the background processes, statistical uncertainties in individual bins of the $m_{\tau\tau}^{\text{vis}}$ distributions are considered as Poissonian nuisance parameters. The uncertainty can reach up to above 40% for some bins in the low-$m_{b\tau\tau}^{\text{vis}}$ categories. The combined effect of all such uncertainties is the dominant systematic uncertainty in this search.

The uncertainties in the jet energy scale [57] affect the overall yields of processes estimated from simulation, as well as their relative contribution to the different categories because the categorization is based on the value of $m_{b\tau\tau}^{\text{vis}}$ for each event. They are functions of the jet p_T and η. The $\vec{p}_T^{\,\text{miss}}$ is recomputed for each variation of the jet energy scale. The uncertainty in the $\vec{p}_T^{\,\text{miss}}$ related to the measurement of the energy that is not clustered in jets [65], is evaluated event-by-event, and is also considered as a shape uncertainty.

Corrections for the efficiency of identification of muons, electrons, and τ_h candidates, are derived from data using tag-and-probe methods, and applied to simulated events as a function of the lepton p_T and η. Uncertainties related to these corrections amount to 5% for τ_h, 2% for electrons, and 2% for muons. Additionally, events with a muon or an electron misidentified as a τ_h candidate have a yield uncertainty of 5%. Trigger scale factors are also estimated with tag-and-probe methods, and their uncertainties in the yields of simulated processes are 1%.

The energy scale of τ_h candidates is corrected per reconstructed decay mode, and the uncertainty of 1.2% per single decay mode is considered as a shape uncertainty. Uncertainties in the energy scales of electrons and muons are also included as shape uncertainties.

Corrections to the efficiency for tagging a b quark jet as a b jet, as well as for mistagging a jet originating from a different flavor, are applied to simulated events on the basis of the generated flavor of the jets. The uncertainties in the scale factors depend on the p_T of the jet and are therefore considered as shape uncertainties. They amount to about 1.5% for jet originating from a b flavor, 5% for a c flavor, and 10% for a light flavor.

The uncertainty in the yield of the backgrounds with jets misidentified as τ_h accounts for possibly different misidentification rates in $Z + \text{jets}$ events (where the misidentification rates are measured), and in $W + \text{jets}$ and QCD multijet events (which dominate the constitution of the reducible background in the signal region), and for differences between data and predicted backgrounds observed in a region enriched in reducible background events by inverting the charge requirement on the τ candidates and removing the m_T and D_ζ selection criteria. This uncertainty amounts to 20%, and is constrained to about 7% after the maximum likelihood fit because of the large number of events contributing to the last $m_{b\tau\tau}^{\text{vis}}$ category. Shape uncertain-

ties are also considered for the backgrounds with jets misidentified as τ_h; they are related to the fit uncertainties of the misidentification probabilities.

The uncertainty in the yield of the QCD multijet background in the eμ background is 20%; the value comes from the uncertainty in the extrapolation factor from the same-sign region to the opposite-sign region. The uncertainty in the W + jets background in this channel also amounts to 20%, and accounts for a potential mismodeling in simulation of the misidentification rate of jets as electrons or muons.

The yield uncertainty of the $t\bar{t}$ background is related to the PDF uncertainty and to the uncertainty associated to the strong coupling constant α_s in the full NNLO plus next-to-next-to-leading-log (NNLL) order calculation of the cross section; it amounts to about 4%. The yield uncertainties for other backgrounds estimated from simulation are taken from recent CMS measurements: 6% for diboson processes [66], 13% for single top quark processes [67], 7% for Z + jets events with at least one b tagged jet in the final state [68]. The uncertainty in the correction of the dilepton p_T distribution is equal to 10% of the size of the correction itself. The uncertainty in the correction of the $m^{vis}_{b\tau\tau}$ distribution is equal to the correction itself, and considered as a shape uncertainty. Uncertainties in the production cross sections and branching fractions for SM Higgs boson processes are taken from Ref. [69]. The uncertainty in the integrated luminosity amounts to 2.5% [70].

7 Results

The $m^{vis}_{\tau\tau}$ distributions in the different channels and categories are shown in Figs. 3–5.

No excess is observed relative to the SM background prediction. Upper limits at 95% CL are set on $\frac{\sigma(h)}{\sigma_{SM}}\mathcal{B}(h \to aa \to 2\tau 2b)$ using the modified frequentist construction CL_s [71], for pseudoscalar masses between 15 and 60 GeV. In this expression, σ_{SM} denotes the production cross section of the Higgs boson predicted in the SM, whereas $\sigma(h)$ is the observed production cross section of the Higgs boson. The limits per channel and for the combination of the three channels are shown in Fig. 6. The most sensitive final state is $\mu\tau_h$. The sensitivity of the eτ_h and eμ channels is approximately equivalent; the first channel suffers from higher trigger thresholds and lower object identification efficiency than $\mu\tau_h$, and the second one suffers from a lower branching fraction than $\mu\tau_h$. At low m_a the eμ final state has a higher signal acceptance than the other final states, especially eτ_h. The limits are best in the intermediate mass range. The low-m_a signals have a lower acceptance because of the overlap of the leptons related to the boost of the pseudoscalar bosons, and of the typically softer lepton and b jet p_T spectra. The high-m_a signals lie in a region where more backgrounds, including Drell-Yan production, contribute, leading also to lower sensitivity than in the intermediate mass region. The categories are complementary over the probed mass range, with the low-$m^{vis}_{b\tau\tau}$ signal regions more sensitive for heavy resonances, and the high-$m^{vis}_{b\tau\tau}$ ones for light resonances.

The combined limit at intermediate mass is as low as 3% on $\mathcal{B}(h \to aa \to 2\tau 2b)$, assuming the SM production cross section and mechanisms for the Higgs boson. Computing the branching fractions of the light pseudoscalar to SM particles as described in Refs. [15, 72], this translates to limits on $\frac{\sigma(h)}{\sigma_{SM}}\mathcal{B}(h \to aa)$ of about 23% in 2HDM+S type II with $\tan\beta > 1$. In the scenario with the highest branching fraction, 2HDM+S type III with $\tan\beta = 2$, the expected limit is as low as 6% at intermediate m_a. Figure 7 shows the observed limits at 95% CL on $\frac{\sigma(h)}{\sigma_{SM}}\mathcal{B}(h \to aa)$ for type III and type IV of 2HDM+S, for which there is a strong dependence with $\tan\beta$. Figure 8 shows the observed limits at 95% CL on $\frac{\sigma(h)}{\sigma_{SM}}\mathcal{B}(h \to aa)$ for a few scenarios of 2HDM+S, assuming

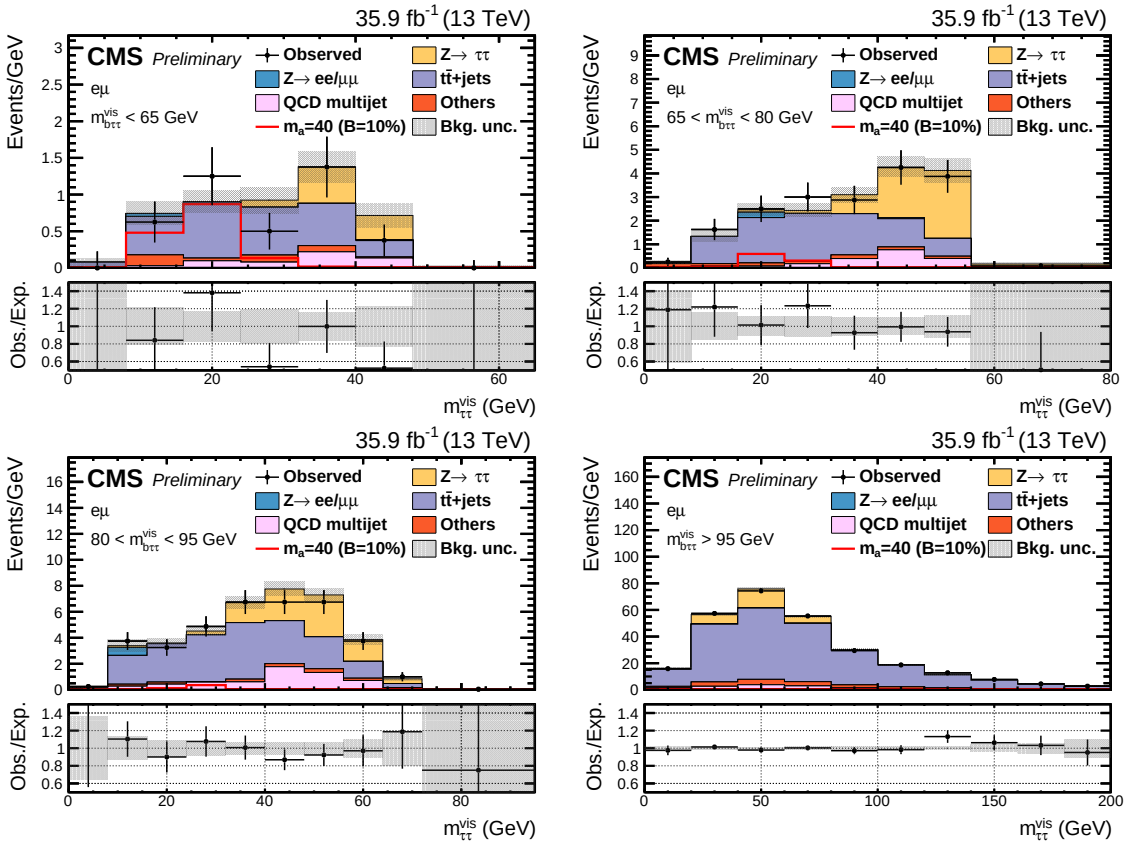

Figure 3: Distributions of $m_{\tau\tau}^{\text{vis}}$ in the four categories of the eμ channel. The "Others" contribution includes events from single top quark, diboson, SM Higgs boson, and W + jets productions. The signal histogram corresponds to the production cross section predicted in the SM for the ggh, VBF, and Vh productions, and assumes $\mathcal{B}(\text{h} \to \text{aa} \to 2\tau 2\text{b}) = 10\%$. The normalization of the predicted background distributions corresponds to the result of the global fit.

the branching fractions of the light pseudoscalar to SM particles computed using Refs. [15, 72]. The limit shown for type II of 2HDM+S is approximately valid for any value of $\tan\beta > 1$.

8 Summary

The first search for exotic decays of the Higgs boson to pairs of light bosons with two b quark jets and two τ leptons in the final state, has been performed with data collected at 13 TeV center-of-mass energy in 2016. This decay channel has a large branching fraction in many models where the couplings to fermions are proportional to the fermion mass, and can be triggered in the dominant gluon fusion production mode because of the presence of light leptons from leptonic τ decays. No excess of events is found on top of the expected standard model background. Upper limits are set on $\mathcal{B}(\text{h} \to \text{aa})$ assuming particular scenarios of two Higgs doublet models augmented with a scalar singlet (2HDM+S); they are, by several factors, the most stringent limits in 2HDM+S type II for $15 < m_{\text{a}} < 62.5$ GeV at the LHC so far.

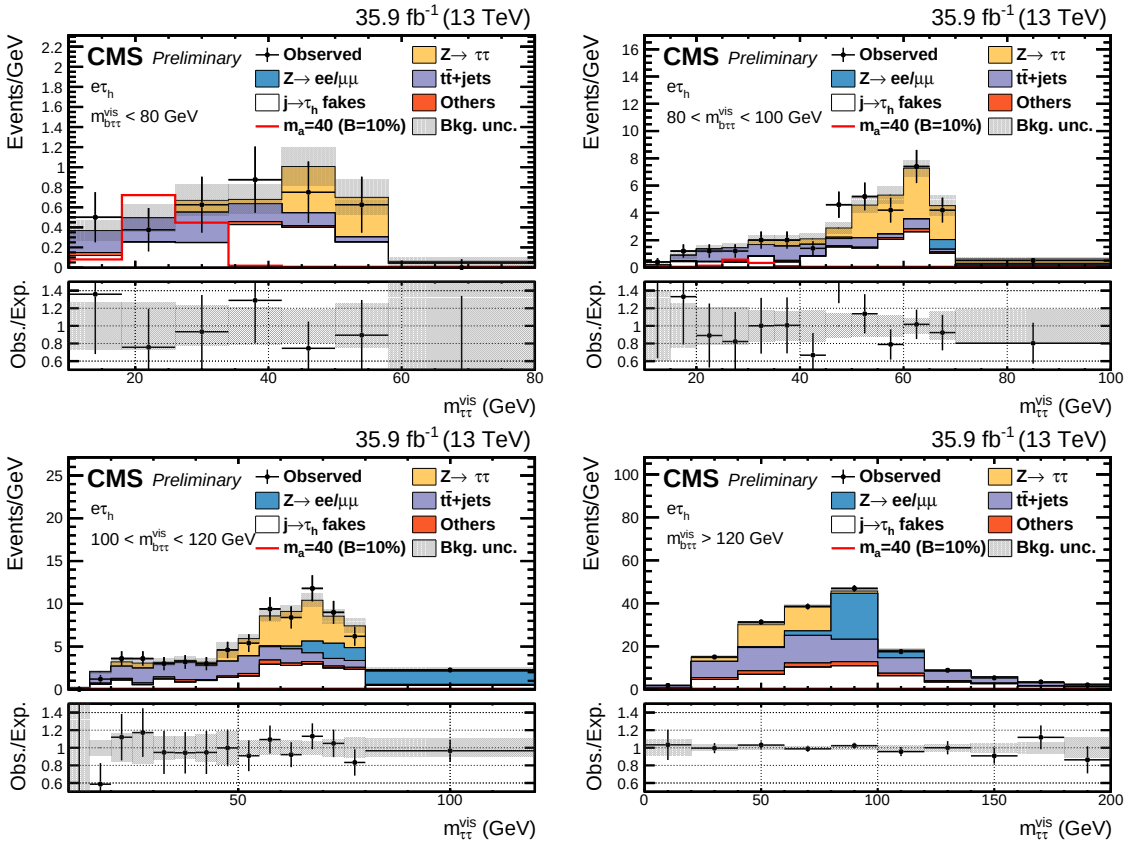

Figure 4: Distributions of $m_{\tau\tau}^{\text{vis}}$ in the four categories of the eτ_{h} channel. The "jet$\rightarrow \tau_{\text{h}}$" contribution includes all events with a jet misidentified as a τ_{h} candidate, whereas the other contributions only include events where the reconstructed τ_{h} corresponds to a τ_{h}, a muon, or an electron, at generated level. The "Others" contribution includes events from single top quark, diboson, and SM Higgs boson productions. The signal histogram corresponds to the production cross section predicted in the SM for the ggh, VBF, and Vh productions, and assumes $\mathcal{B}(\text{h} \rightarrow \text{aa} \rightarrow 2\tau 2\text{b}) = 10\%$. The normalization of the predicted background distributions corresponds to the result of the global fit.

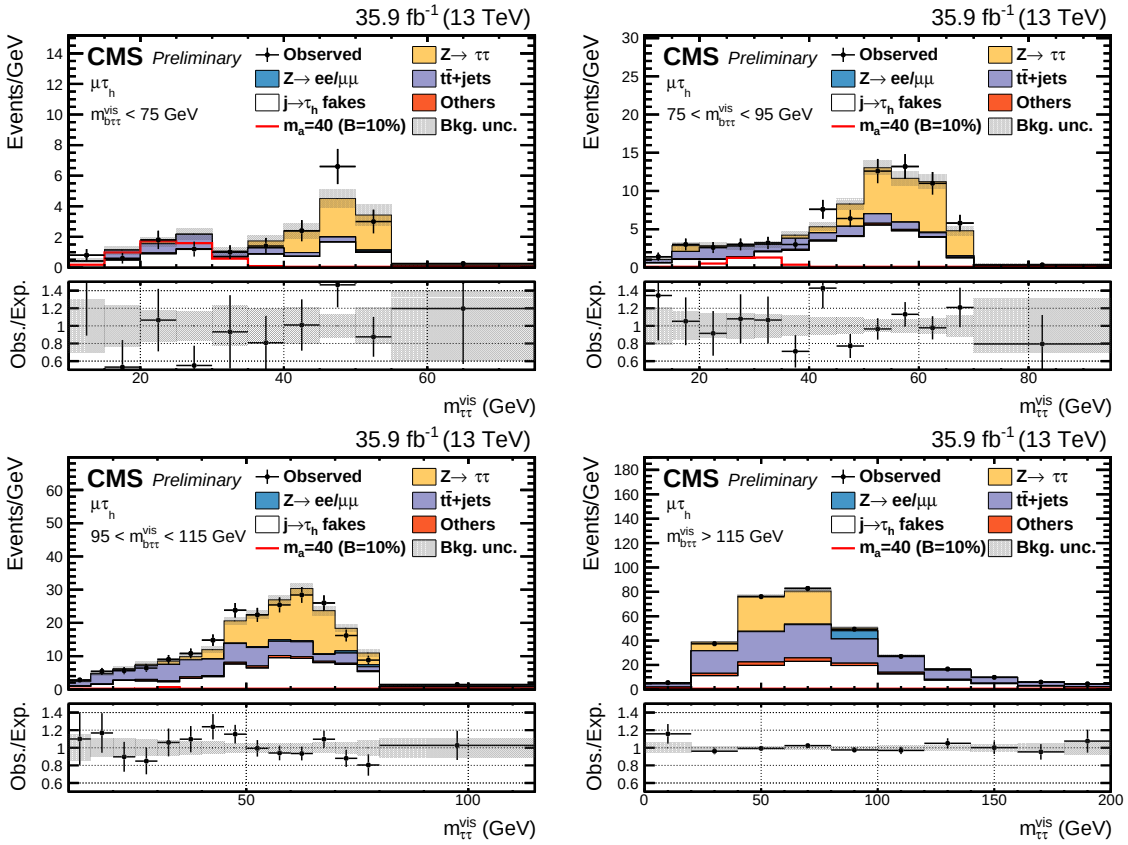

Figure 5: Distributions of $m_{\tau\tau}^{\text{vis}}$ in the four categories of the $\mu\tau_{\text{h}}$ channel. The "jet$\rightarrow\ \tau_{\text{h}}$" contribution includes all events with a jet misidentified as a τ_{h} candidate, whereas the other contributions only include events where the reconstructed τ_{h} corresponds to a τ_{h}, a muon, or an electron, at generated level. The "Others" contribution includes events from single top quark, diboson, and SM Higgs boson productions. The signal histogram corresponds to the production cross section predicted in the SM for the ggh, VBF, and Vh productions, and assumes $\mathcal{B}(\text{h} \rightarrow \text{aa} \rightarrow 2\tau 2\text{b}) = 10\%$. The normalization of the predicted background distributions corresponds to the result of the global fit.

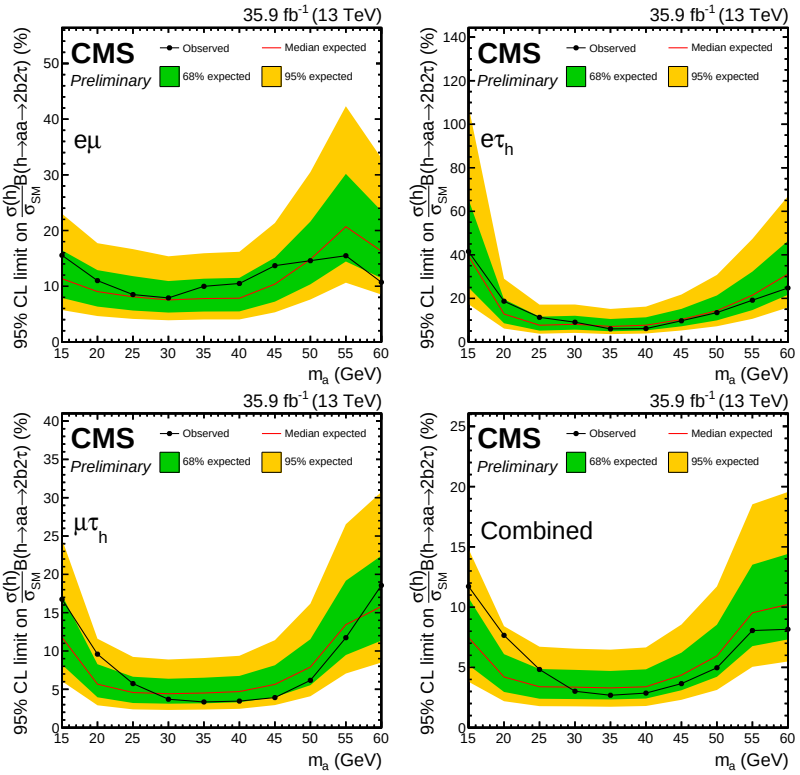

Figure 6: Expected and observed 95% CL limits on $\frac{\sigma(\mathrm{h})}{\sigma_{SM}}\mathcal{B}(\mathrm{h} \rightarrow \mathrm{aa} \rightarrow 2\tau 2\mathrm{b})$ in %. The eμ results are shown in the top left panel, eτ_h in the top right, $\mu\tau_\mathrm{h}$ in the bottom left, and the combination in the bottom right. The inner (green) band and the outer (yellow) band indicate the regions containing 68 and 95%, respectively, of the distribution of limits expected under the background-only hypothesis.

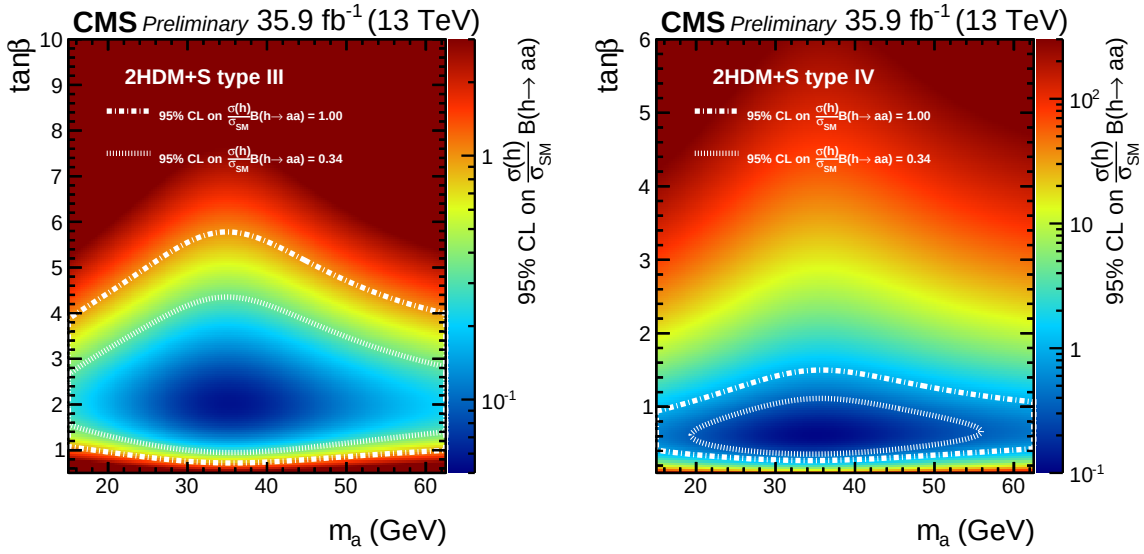

Figure 7: Observed 95% CL on $\frac{\sigma(\mathrm{h})}{\sigma_{SM}}\mathcal{B}(\mathrm{h} \to \mathrm{aa})$ in 2HDM+S of type III (left), and type IV (right). The contours corresponding to a 95% CL exclusion of $\frac{\sigma(\mathrm{h})}{\sigma_{SM}}\mathcal{B}(\mathrm{h} \to \mathrm{aa}) = 1.00$ and 0.34 are drawn with dashed lines. The number 34% corresponds to the limit on the branching fraction of the Higgs boson to BSM particles at the 95% CL obtained with data collected at a center-of-mass energy of 8 TeV by the CMS and ATLAS experiments [10].

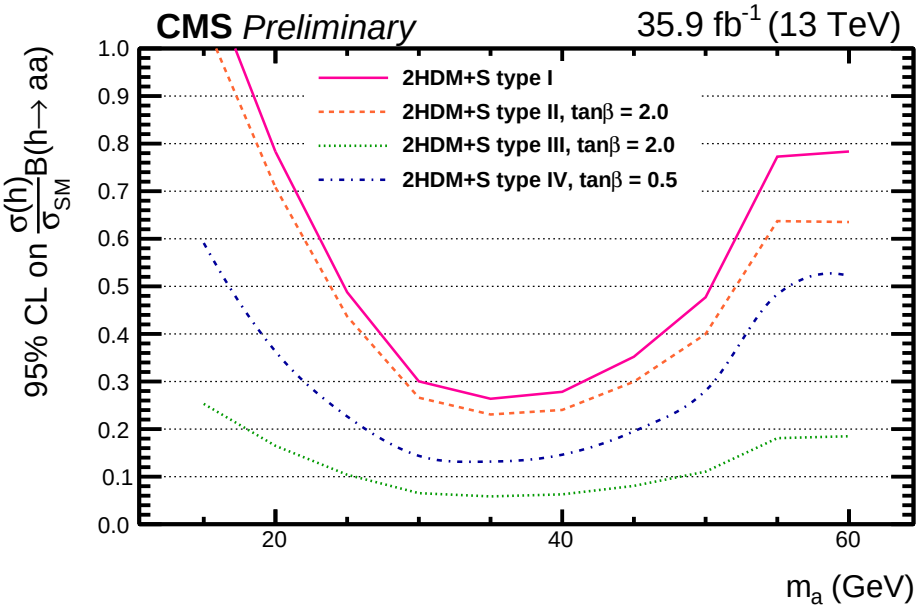

Figure 8: Observed 95% CL on $\frac{\sigma(\mathrm{h})}{\sigma_{SM}}\mathcal{B}(\mathrm{h} \to \mathrm{aa})$ for various scenarios of 2HDM+S.

References

[1] F. Englert and R. Brout, "Broken symmetry and the mass of gauge vector mesons", *Phys. Rev. Lett.* **13** (1964) 321, doi:10.1103/PhysRevLett.13.321.

[2] P. W. Higgs, "Broken symmetries, massless particles and gauge fields", *Phys. Lett.* **12** (1964) 132, doi:10.1016/0031-9163(64)91136-9.

[3] P. W. Higgs, "Broken symmetries and the masses of gauge bosons", *Phys. Rev. Lett.* **13** (1964) 508, doi:10.1103/PhysRevLett.13.508.

[4] G. S. Guralnik, C. R. Hagen, and T. W. B. Kibble, "Global conservation laws and massless particles", *Phys. Rev. Lett.* **13** (1964) 585, doi:10.1103/PhysRevLett.13.585.

[5] P. W. Higgs, "Spontaneous symmetry breakdown without massless bosons", *Phys. Rev.* **145** (1966) 1156, doi:10.1103/PhysRev.145.1156.

[6] T. W. B. Kibble, "Symmetry Breaking in Non-Abelian Gauge Theories", *Phys. Rev.* **155** (1967) 1554, doi:10.1103/PhysRev.155.1554.

[7] ATLAS Collaboration, "Observation of a new particle in the search for the Standard Model Higgs boson with the ATLAS detector at the LHC", *Phys. Lett. B* **716** (2012) doi:10.1016/j.physletb.2012.08.020, arXiv:1207.7214.

[8] CMS Collaboration, "Observation of a new boson at a mass of 125 GeV with the CMS experiment at the LHC", *Phys. Lett. B* **716** (2012) doi:10.1016/j.physletb.2012.08.021, arXiv:1207.7235.

[9] CMS Collaboration, "Observation of a new boson with mass near 125 GeV in pp collisions at $\sqrt{s}$ = 7 and 8 TeV", *JHEP* **06** (2013) 081, doi:10.1007/JHEP06(2013)081, arXiv:1303.4571.

[10] ATLAS and CMS Collaborations, "Measurements of the Higgs boson production and decay rates and constraints on its couplings from a combined ATLAS and CMS analysis of the LHC pp collision data at $\sqrt{s} = 7$ and 8 TeV", *JHEP* **08** (2016) 045, doi:10.1007/JHEP08(2016)045, arXiv:1606.02266.

[11] ATLAS and CMS Collaborations, "Combined measurement of the Higgs boson mass in pp collisions at $\sqrt{s} = 7$ and 8 TeV with the ATLAS and CMS experiments", *Phys. Rev. Lett.* **114** (2015) 191803, doi:10.1103/PhysRevLett.114.191803, arXiv:1503.07589.

[12] R. Dermisek and J. F. Gunion, "Escaping the large fine tuning and little hierarchy problems in the next to minimal supersymmetric model and $h \to aa$ decays", *Phys. Rev. Lett.* **95** (2005) 041801, doi:10.1103/PhysRevLett.95.041801, arXiv:hep-ph/0502105.

[13] R. Dermisek and J. F. Gunion, "The NMSSM close to the R-symmetry limit and naturalness in $h \to aa$ decays for $m_a < 2m_b$", *Phys. Rev. D* **75** (2007) 075019, doi:10.1103/PhysRevD.75.075019, arXiv:hep-ph/0611142.

[14] S. Chang, R. Dermisek, J. F. Gunion, and N. Weiner, "Nonstandard Higgs boson decays", *Ann. Rev. Nucl. Part. Sci.* **58** (2008) 75, doi:10.1146/annurev.nucl.58.110707.171200, arXiv:0801.4554.

[15] D. Curtin et al., "Exotic decays of the 125 GeV Higgs boson", *Phys. Rev. D* **90** (2014) 075004, doi:10.1103/PhysRevD.90.075004, arXiv:1312.4992.

[16] CMS Collaboration, "Search for neutral mssm higgs bosons decaying to a pair of tau leptons in pp colllisions", *JHEP* **10** (2014) 160, doi:10.1007/JHEP10(2014)160, arXiv:1408.3316.

[17] CMS Collaboration, "Search for neutral MSSM Higgs bosons decaying into a pair of bottom quarks", *JHEP* **11** (2015) 071, doi:10.1007/JHEP11(2015)071, arXiv:1506.08329.

[18] CMS Collaboration, "Search for neutral MSSM Higgs bosons decaying to $\mu^+\mu^-$ in pp collisions at $\sqrt{s} = 7$ and 8 TeV", *Phys. Lett. B* **752** (2016) 221, doi:10.1016/j.physletb.2015.11.042, arXiv:1508.01437.

[19] CMS Collaboration, "Search for a charged Higgs boson in pp collisions at $\sqrt{s} = 8$ TeV", *JHEP* **11** (2015) 018, doi:10.1007/JHEP11(2015)018, arXiv:1508.07774.

[20] CMS Collaboration, "Search for Higgs boson pair production in events with two bottom quarks and two tau leptons in proton-proton collisions at sqrt(s) = 13 TeV", arXiv:1707.02909.

[21] CMS Collaboration, "Searches for a heavy scalar boson H decaying to a pair of 125 GeV Higgs bosons hh or for a heavy pseudoscalar boson A decaying to Zh, in the final states with $h \to \tau\tau$", *Phys. Lett. B* **755** (2016) 217, doi:10.1016/j.physletb.2016.01.056, arXiv:1510.01181.

[22] S. Heinemeyer, O. Stal, and G. Weiglein, "Interpreting the LHC Higgs search results in the MSSM", *Phys. Lett. B* **710** (2012) 201, doi:10.1016/j.physletb.2012.02.084, arXiv:1112.3026.

[23] G. C. Branco et al., "Theory and phenomenology of two-Higgs-doublet models", *Phys. Rep.* **516** (2012) 1, doi:10.1016/j.physrep.2012.02.002, arXiv:1106.0034.

[24] S. Ramos-Sanchez, "The mu-problem, the nmssm and string theory", *Fortsch.Phys.58:748-752,2010* **58** (2010) 748–752, doi:10.1002/prop.201000058, arXiv:1003.1307.

[25] CMS Collaboration, "Search for light bosons in decays of the 125 GeV Higgs boson in proton-proton collisions at $\sqrt{s} = 8$ TeV", *JHEP* **10** (2017) 076, doi:10.1007/JHEP10(2017)076, arXiv:1701.02032.

[26] CMS Collaboration, "Search for a very light NMSSM Higgs boson produced in decays of the 125 GeV scalar boson and decaying into τ leptons in pp collisions at $\sqrt{s} = 8$ TeV", *JHEP* **01** (2016) 079, doi:10.1007/JHEP01(2016)079, arXiv:1510.06534.

[27] CMS Collaboration, "A search for pair production of new light bosons decaying into muons", *Phys. Lett. B* **752** (2016) 146, doi:10.1016/j.physletb.2015.10.067, arXiv:1506.00424.

[28] ATLAS Collaboration, "Search for the Higgs boson produced in association with a W boson and decaying to four b-quarks via two spin-zero particles in pp collisions at 13 TeV with the ATLAS detector", *Eur. Phys. J. C* **76** (2016) 605, doi:10.1140/epjc/s10052-016-4418-9, arXiv:1606.08391.

[29] ATLAS Collaboration, "Search for new light gauge bosons in Higgs boson decays to four-lepton final states in pp collisions at $\sqrt{s} = 8$ TeV with the ATLAS detector at the LHC", *Phys. Rev. D* **92** (2015) 092001, doi:10.1103/PhysRevD.92.092001, arXiv:1505.07645.

[30] ATLAS Collaboration, "Search for Higgs boson decays to beyond-the-Standard-Model light bosons in four-lepton events with the ATLAS detector at $\sqrt{s} = 13$ TeV", arXiv:1802.03388.

[31] ATLAS Collaboration, "Search for new phenomena in events with at least three photons collected in pp collisions at $\sqrt{s} = 8$ TeV with the ATLAS detector", *Eur. Phys. J. C* **76** (2016) 210, doi:10.1140/epjc/s10052-016-4034-8, arXiv:1509.05051.

[32] ATLAS Collaboration, "Search for Higgs bosons decaying to aa in the $\mu\mu\tau\tau$ final state in pp collisions at $\sqrt{s} = 8$ TeV with the ATLAS experiment", *Phys. Rev. D* **92** (2015) 052002, doi:10.1103/PhysRevD.92.052002, arXiv:1505.01609.

[33] CMS Collaboration, "The CMS trigger system", *JINST* **12** (2017) P01020, doi:10.1088/1748-0221/12/01/P01020, arXiv:1609.02366.

[34] CMS Collaboration, "The CMS experiment at the CERN LHC", *JINST* **3** (2008) S08004, doi:10.1088/1748-0221/3/08/S08004.

[35] J. Alwall et al., "The automated computation of tree-level and next-to-leading order differential cross sections, and their matching to parton shower simulations", *JHEP* **07** (2014) 079, doi:10.1007/JHEP07(2014)079, arXiv:1405.0301.

[36] J. Alwall et al., "Comparative study of various algorithms for the merging of parton showers and matrix elements in hadronic collisions", *Eur. Phys. J. C* **53** (2008) 473, doi:10.1140/epjc/s10052-007-0490-5, arXiv:0706.2569.

[37] P. Nason, "A new method for combining NLO QCD with shower Monte Carlo algorithms", *JHEP* **11** (2004) 040, doi:10.1088/1126-6708/2004/11/040, arXiv:hep-ph/0409146.

[38] S. Frixione, P. Nason, and C. Oleari, "Matching NLO QCD computations with parton shower simulations: the POWHEG method", *JHEP* **11** (2007) 070, doi:10.1088/1126-6708/2007/11/070, arXiv:0709.2092.

[39] S. Alioli, P. Nason, C. Oleari, and E. Re, "A general framework for implementing NLO calculations in shower Monte Carlo programs: the POWHEG BOX", *JHEP* **06** (2010) 043, doi:10.1007/JHEP06(2010)043, arXiv:1002.2581.

[40] S. Alioli et al., "Jet pair production in POWHEG", *JHEP* **04** (2011) 081, doi:10.1007/JHEP04(2011)081, arXiv:1012.3380.

[41] S. Alioli, P. Nason, C. Oleari, and E. Re, "NLO Higgs boson production via gluon fusion matched with shower in POWHEG", *JHEP* **04** (2009) 002, doi:10.1088/1126-6708/2009/04/002, arXiv:0812.0578.

[42] G. Luisoni, P. Nason, C. Oleari, and F. Tramontano, "$HW^{\pm}/HZ + 0$ and 1 jet at NLO with the POWHEG BOX interfaced to GoSam and their merging within MiNLO", *JHEP* **10** (2013) 083, doi:10.1007/JHEP10(2013)083, arXiv:1306.2542.

[43] T. Sjostrand et al., "An introduction to PYTHIA 8.2", *Comput. Phys. Commun.* **191** (2015) 159, doi:10.1016/j.cpc.2015.01.024, arXiv:1410.3012.

[44] CMS Collaboration, "Event generator tunes obtained from underlying event and multiparton scattering measurements", *Eur. Phys. J. C* **76** (2016) 155, doi:10.1140/epjc/s10052-016-3988-x, arXiv:1512.00815.

[45] M. Czakon, P. Fiedler, and A. Mitov, "Total Top-Quark Pair-Production Cross Section at Hadron Colliders Through O(α_S^4)", *Phys. Rev. Lett.* **110** (2013) 252004, doi:10.1103/PhysRevLett.110.252004, arXiv:1303.6254.

[46] M. Czakon and A. Mitov, "Top++: A Program for the Calculation of the Top-Pair Cross-Section at Hadron Colliders", *Comput. Phys. Commun.* **185** (2014) 2930, doi:10.1016/j.cpc.2014.06.021, arXiv:1112.5675.

[47] S. Alekhin et al., "The PDF4LHC Working Group Interim Report", (2011). arXiv:1101.0536.

[48] M. Botje et al., "The PDF4LHC Working Group Interim Recommendations", (2011). arXiv:1101.0538.

[49] H.-L. Lai et al., "New parton distributions for collider physics", *Phys. Rev. D* **82** (2010) 074024, doi:10.1103/PhysRevD.82.074024, arXiv:1007.2241.

[50] J. Gao et al., "CT10 next-to-next-to-leading order global analysis of QCD", *Phys. Rev. D* **89** (2014) 033009, doi:10.1103/PhysRevD.89.033009, arXiv:1302.6246.

[51] NNPDF Collaboration, "Parton distributions with LHC data", *Nucl. Phys. B* **867** (2013) 244, doi:10.1016/j.nuclphysb.2012.10.003, arXiv:1207.1303.

[52] GEANT4 Collaboration, "GEANT4 — a simulation toolkit", *Nucl. Instrum. Meth. A* **506** (2003) 250, doi:10.1016/S0168-9002(03)01368-8.

[53] CMS Collaboration, "Particle-flow reconstruction and global event description with the CMS detector", (2017). arXiv:1706.04965. Submitted to J. Instrum.

[54] M. Cacciari, G. P. Salam, and G. Soyez, "The anti-k_t jet clustering algorithm", *JHEP* **04** (2008) 063, doi:10.1088/1126-6708/2008/04/063, arXiv:0802.1189.

[55] M. Cacciari, G. P. Salam, and G. Soyez, "FastJet user manual", *Eur. Phys. J. C* **72** (2012) 1896, doi:10.1140/epjc/s10052-012-1896-2, arXiv:1111.6097.

[56] M. Cacciari and G. P. Salam, "Dispelling the N^3 myth for the k_t jet-finder", *Phys. Lett. B* **641** (2006) 57, doi:10.1016/j.physletb.2006.08.037, arXiv:hep-ph/0512210.

[57] CMS Collaboration, "Determination of jet energy calibration and transverse momentum resolution in CMS", *JINST* **6** (2011) 11002, doi:10.1088/1748-0221/6/11/P11002, arXiv:1107.4277.

[58] CMS Collaboration, "Identification of heavy-flavour jets with the CMS detector in pp collisions at 13 TeV", arXiv:1712.07158.

[59] CMS Collaboration, "Reconstruction and identification of τ lepton decays to hadrons and ν_τ at CMS", *JINST* **11** (2016) P01019, doi:10.1088/1748-0221/11/01/P01019, arXiv:1510.07488.

[60] CMS Collaboration, "Performance of reconstruction and identification of tau leptons in their decays to hadrons and tau neutrino in LHC Run-2", CMS Physics Analysis Summary CMS-PAS-TAU-16-002, 2016.

[61] CMS Collaboration, "Performance of electron reconstruction and selection with the CMS detector in proton-proton collisions at $\sqrt{s} = 8$ TeV", *JINST* **10** (2015) P06005, doi:10.1088/1748-0221/10/06/P06005, arXiv:1502.02701.

[62] CMS Collaboration, "Performance of CMS muon reconstruction in pp collision events at $\sqrt{s} = 7$ TeV", *JINST* **7** (2012) P10002, doi:10.1088/1748-0221/7/10/P10002, arXiv:1206.4071.

[63] CMS Collaboration, "Search for neutral MSSM Higgs bosons decaying to a pair of tau leptons in pp collisions", *JHEP* **10** (2014) 160, doi:10.1007/JHEP10(2014)160, arXiv:1408.3316.

[64] J. S. Conway, "Incorporating nuisance parameters in likelihoods for multisource spectra", in *Proceedings of PHYSTAT 2011 Workshop on Statistical Issues Related to Discovery Claims in Search Experiments and Unfolding*, p. 115. CERN-2011-006, 2011.

[65] CMS Collaboration, "Performance of missing transverse momentum reconstruction algorithms in proton-proton collisions at $\sqrt{s} = 8$ TeV with the CMS detector", CMS Physics Analysis Summary CMS-PAS-JME-12-002, 2012.

[66] CMS Collaboration, "Measurements of the pp→ZZ production cross section and the Z→ 4ℓ branching fraction, and constraints on anomalous triple gauge couplings at $\sqrt{s} =$ 13 TeV", arXiv:1709.08601. Submitted to Eur. Phys. J. C.

[67] CMS Collaboration, "Cross section measurement of t-channel single top quark production in pp collisions at $\sqrt{s} = 13$ TeV", *Phys. Lett. B* **772** (2017) 752, doi:10.1016/j.physletb.2017.07.047, arXiv:1610.00678.

[68] CMS Collaboration, "Measurements of the associated production of a Z boson and b jets in pp collisions at $\sqrt{s} = 8$ TeV", *Eur. Phys. J. C* **77** (2017), no. 11, 751, doi:10.1140/epjc/s10052-017-5140-y, arXiv:1611.06507.

[69] D. de Florian et al., "Handbook of LHC Higgs cross sections: 4. deciphering the nature of the Higgs sector", CERN Report CERN-2017-002-M, 2016. doi:10.23731/CYRM-2017-002, arXiv:1610.07922.

[70] CMS Collaboration, "CMS luminosity measurements for the 2016 data taking period", CMS Physics Analysis Summary CMS-PAS-LUM-17-001, 2017.

[71] T. Junk, "Confidence level computation for combining searches with small statistics", *Nucl. Instrum. Meth. A* **434** (1999) 435, doi:10.1016/S0168-9002(99)00498-2, arXiv:hep-ex/9902006.

[72] A. Djouadi, "The anatomy of electro-weak symmetry breaking. I: the Higgs boson in the standard model", *Phys. Rep.* **457** (2008) 1, doi:10.1016/j.physrep.2007.10.004, arXiv:hep-ph/0503172.